

Nanoporous Polymer Reflectors for Organic Solar Cells

Shudong Yu, Bing Guo, Siegbert Johnsen, Gabriele Wiegand, Uli Lemmer, Xia Guo, Maojie Zhang, Yongfang Li, Christian Sprau, Hendrik Hölscher, Alexander Colsmann,* and Guillaume Gomard*

Due to their high transparency, electrodes fabricated from conductive polymers are often implemented in semitransparent organic solar cells. Opaque solar cells usually employ metal back electrodes with high reflectivity for best photon confinement in the light-harvesting layer. Herein, a bilayer back electrode comprising conductive polymers and nanofoamed poly(methyl methacrylate) (PMMA) is investigated, the latter of which creates diffuse reflection of the incoming light. By tuning the thickness of the nanofoamed PMMA layer, absorption and transmission of the solar cells can be tailored from opaque to vastly transparent. Due to its diffusive character, this versatile electrode enhances the light absorption in the wavelength regimes with lower absorption coefficient. The solar cells are particularly suited for deployment in frosted window applications.

1. Introduction

Among the emerging photovoltaic technologies, organic solar cells (OSCs) stand out with their design flexibility in color and shape, their lightweight, their mechanical flexibility, their potential sustainability all along the value chain, and their optional semitransparency.^[1–7] Recently, power conversion efficiencies (PCEs) of OSCs have surpassed 18%, enabled by the advent of nonfullerene acceptors, by tuning of the microstructure of the bulk-heterojunction, by tailoring the spectral absorption, and by smart device design.^[8] Printing technologies, including inkjet


printing, doctor blading, and roll-to-roll printing, are widely considered toward large-scale fabrication and commercialization of OSCs.^[1] Other than the light-harvesting layers, charge carrier transport layers and electrodes must also be solution processable for any fully integrated printing process. While the front electrode can be printed from conductive polymers, the back electrode is envisaged to be printed from silver inks, in order to use its back reflections for enhanced light harvesting inside the device. The feasibility of printing and the sustainability of materials would gain from the implementation of back electrodes also comprising conductive

polymers instead of silver or using only small amounts thereof. Earlier works have shown that the substitution of rear metal electrodes by highly conductive polymers is feasible,^[9,10] and that the limited conductivity of polymer electrodes can be mitigated by incorporating silver nanowires while preserving the mechanical robustness of the solar cell.^[10] Although this concept is of great use to realize semitransparent solar cells, e.g., for window or façade integration, the much smaller reflectance of the polymer electrode versus the commonly used metal electrode reduces light harvesting and hence the PCE of OSCs. To mitigate these transmission losses and to harvest those unabsorbed photons,

S. Yu, B. Guo, U. Lemmer, A. Colsmann, G. Gomard
Light Technology Institute
Karlsruhe Institute of Technology (KIT)
76131 Karlsruhe, Germany
E-mail: alexander.colsmann@kit.edu; guillaume.gomard@zeiss.com

S. Yu
Guangdong Provincial Key Laboratory of Technique and Equipment for
Macromolecular Advanced Manufacturing
South China University of Technology (SCUT)
Guangzhou 510640, China

B. Guo, C. Sprau, A. Colsmann
Material Research Center for Energy Systems
Karlsruhe Institute of Technology (KIT)
76131 Karlsruhe, Germany

 The ORCID identification number(s) for the author(s) of this article can be found under <https://doi.org/10.1002/ente.202100676>.

© 2021 The Authors. Energy Technology published by Wiley-VCH GmbH. This is an open access article under the terms of the Creative Commons Attribution License, which permits use, distribution and reproduction in any medium, provided the original work is properly cited.

DOI: 10.1002/ente.202100676

B. Guo, X. Guo, M. Zhang, Y. Li
Laboratory of Advanced Optoelectronic Materials
College of Chemistry
Chemical Engineering and Materials Science
Soochow University
Suzhou 215123, China

S. Johnsen, G. Wiegand
Institute of Catalysis Research and Technology
Karlsruhe Institute of Technology (KIT)
76344 Eggenstein-Leopoldshafen, Karlsruhe, Germany

U. Lemmer, H. Hölscher, G. Gomard
Institute for Microstructure Technology
Karlsruhe Institute of Technology (KIT)
76344 Eggenstein-Leopoldshafen, Karlsruhe, Germany

Y. Li
CAS Key Laboratory of Organic Solids
Institute of Chemistry
Beijing National Laboratory for Molecular Sciences
Chinese Academy of Sciences
Beijing 100190, China

various methods have been proposed, including multilayer distributed Bragg reflectors,^[11–16] pyramidal rear reflectors,^[17] and cholesteric liquid crystal reflectors.^[18] Light harvesting can also be enhanced by prolonging the way of the photons through the device by light scattering. Tang et al. proposed a pigmented dielectric reflector consisting of titania nanoparticles embedded within a polydimethylsiloxane matrix to be implemented as a cost-effective light-trapping structure for OSCs.^[19] The use of pigmented dielectric reflectors for PV was first explored 20 years ago by Cotter et al.^[20] in thin silicon solar cells and further used to enhance the PCE of thin-film silicon devices.^[21] In order to increase the light scattering efficiency of dielectric reflectors and to increase the refractive index contrast, the host material was further removed using snow globe coating.^[22] The spacing between aggregates of titania nanoparticles filled with air that exhibits dimensions comparable to the wavelength of light, thus resulted in longer optical paths and some PCE enhancement.^[23] Such nanoporous reflectors can also be realized from polymer networks, where light scattering depends on the morphology of the porous network in the polymer matrix, which can be tuned through different processes, including electrospinning or phase-separation methods.^[24–27]

In this study, we demonstrate that the reflective rear metal electrode in an OSC can be replaced by a combination of a conductive polymer electrode and a reflecting (light scattering) nanoporous polymer film, the latter of which is fabricated by supercritical CO₂ foaming. The process is versatile, cost-effective, reproducible, rapid, and industrially viable. It can be used with various polymers and generates mechanically stable nanoporous films. In a previous study, we reported that foamed polymer films are highly reflecting over the visible and near-infrared spectrum.^[28] Upon variation of the thickness of the foamed films, the ratio of reflected/transmitted light can be tuned easily. We take advantage of this effect to tailor light management in OSCs for their light harvesting properties and their transmittance, depending on the envisaged application.

2. Results and Discussion

2.1. Device Design

To explore the photovoltaic performance enhancement brought by the nanoporous polymer reflectors, we have chosen the solar cell architecture that is depicted in **Figure 1a**, comprising indium tin oxide (ITO), zinc oxide (ZnO), a blend layer of the conjugated polymer donor poly[[4,8-bis[5-(2-ethylhexyl)-2-thienyl]benzo[1,2-b:4,5-b']dithiophene-2,6-diyl]-2,5-thiophenediyl[5,7-bis(2-ethylhexyl)-4,8-dioxo-4H,8H-benzo[1,2-c:4,5-c']dithiophene-1,3-diyl]] (PBDB-T) and the molecular acceptor 3,9-bis(2-methylene-(3-(1,1-dicyanomethylene)-indanone))-5,5,11,11-tetrakis(4-hexylphenyl)dithieno[2,3-d:2',3'-d']-s-indaceno[1,2-b:5,6-b']dithiophene (ITIC) as well as a poly(3,4-ethylenedioxythiophene):poly(styrene-sulfonate) (PEDOT:PSS) counter electrode. PBDB-T:ITIC was chosen for light harvesting due to its high efficiency and its excellent thermal stability.^[29] The surface resistivity of the 70 nm-thick polymer electrode was reduced to 35 Ω sq⁻¹ by the incorporation of silver nanowires (AgNW) that were readily dispersed in the as-purchased PEDOT:PSS formulation (HYE).^[10] The rear reflector comprises a volumetric network of light scattering nanopores and was mechanically attached to the PEDOT:PSS:AgNW electrode. The incoming light propagates through the glass substrate first. After passing through the device, the unabsorbed photons are retro-reflected into the light-harvesting layer, eventually enhancing the overall absorption and the PCE of the solar cell. For reference, we mechanically attached an electrically isolated silver (Ag) layer to the PEDOT:PSS:AgNW electrode, mimicking the reflectance of a metal electrode while not changing the conductivity of the electrode, hence separating the optical effects from the electronic effects.

2.2. Optical Properties of the Nanoporous Polymer Reflectors

At the outset of our study, we foamed a commercially available poly(methyl methacrylate) (PMMA) sample with a thickness of

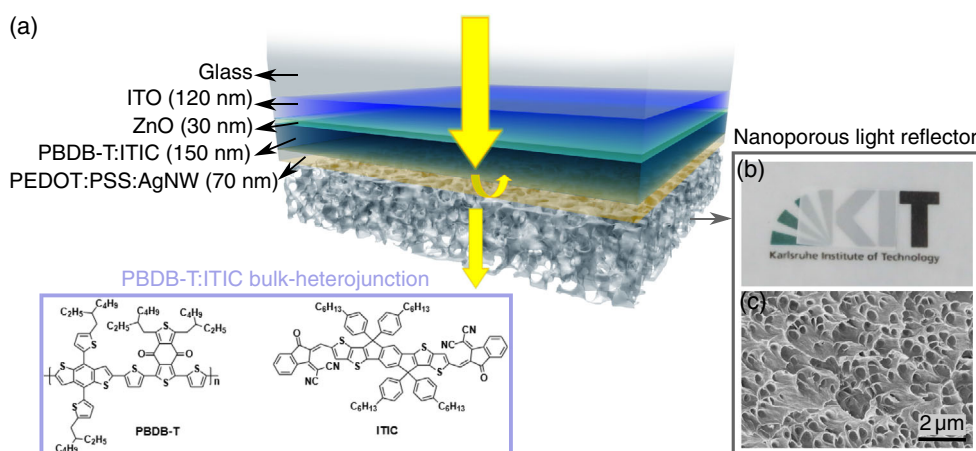


Figure 1. Nanoporous polymer films behind the rear polymer electrode are used to tailor the reflectivity of the electrode and hence to tune the transmission and the PCE of the OSCs. a) Illustration of the solar cell architecture. The foamed polymer film has a thin skin layer on both sides which was omitted in this illustration for better visualization. Inset: molecular structures of the bulk-heterojunction components. b) Photograph of a nanoporous reflector with a nominal thickness of 20 μm. The logo is reproduced with permission from Karlsruhe Institute of Technology. c) Cross-sectional scanning electron microscopy image of a representative nanoporous reflector with a thickness of 20 μm revealing the dense nanopore assembly (average diameter of the pores $d = 320 \pm 40$ nm).

500 μm . The foamed sample exhibits an almost 100% broadband reflection by light scattering (close to 0% transmission) over the wavelength range of interest and hence is an effective back reflector for opaque solar cells. **Figure 2** depicts the light reflectance of this 500 μm -thick sample with the optical properties of a typical opaque silver electrode. We note that the decrease of reflectance below 400 nm can be attributed to UV absorption of additives in certain types of commercial PMMA.

In order to tailor the translucency of the solar cells, we fabricated a series of nanoporous PMMA reflectors following the process described in our previous work.^[30] The nanoporous reflectors were produced individually by foaming of PMMA with supercritical CO_2 at 50 MPa for 1 min. This facile process enables the rapid and homogeneous introduction of nanopores (here with an average diameter of 320 ± 40 nm) into the PMMA films while maintaining closed and planar film surfaces (i.e., free from pores), hence facilitating their mechanical and optical coupling to the solar cells. The coupling of the PMMA reflectors was further facilitated by their mechanical flexibility due to their low thickness between 10 and 50 μm . To tailor the translucency of the nanoporous reflectors, we deliberately maintained the foaming parameters but adjusted the thickness of the PMMA film prior to foaming. Notably, similar effects can be achieved by varying the foaming parameters and hence the morphology of the porous network (including the density and the average diameter of the nanopores) while maintaining the film thickness.

Four nanoporous reflectors were fabricated by gradually increasing the thickness of the PMMA film. The target thicknesses of the pristine PMMA films (i.e., before foaming) were 10, 20, 30, and 50 μm (thicknesses achieved: 8.9, 19.2, 31.8, and 52 μm). Upon foaming, i.e., the incorporation of CO_2 , the above listed samples inflated to 9.3, 21.5, 35.5, and 61.1 μm . The relative increase of the sample thickness toward thicker samples upon foaming can be attributed to the formation of a skin layer without pores where the CO_2 diffuses out of the sample rather quickly. Hence, thin samples hardly gain in thickness during the foaming process, whereas thick samples inflate

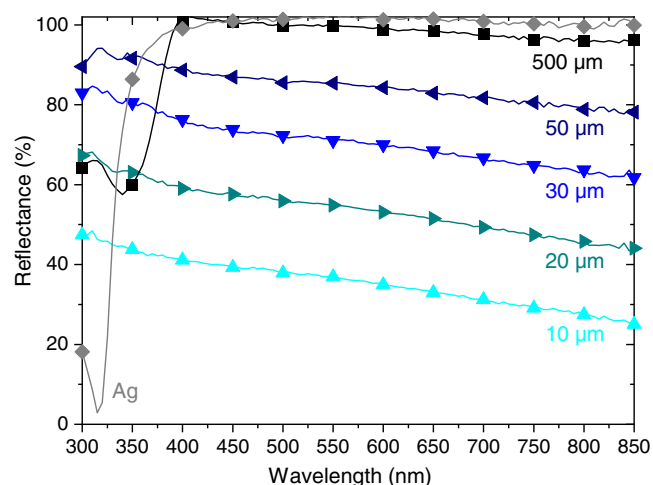


Figure 2. Wavelength-dependent reflectance of the nanoporous reflectors with different thicknesses. For reference, the reflectance of Ag (100 nm) and foamed PMMA (500 μm) reflectors are included. For better readability, only one out of ten data points is marked with a symbol.

significantly (relative thickness gain: 4%, 12%, 12%, and 18%). We note that the CO_2 diffusion and skin-layer formation produce a nonhomogenous vertical gas inclusion profile throughout the sample, which is difficult to describe quantitatively. Figure 2 depicts the reflectance spectra of the foamed samples in comparison to the Ag electrode (thickness: 100 nm) and the 500 μm foamed commercial reference. The spectra of the nanoporous reflectors are essentially featureless, yet display a spectral dependency with a higher reflectance toward smaller wavelengths, comparable to the size of the nanopores, which induce complex multiscattering effects.

The left side of **Figure 3** depicts the series of nanofoamed reflectors with different thicknesses, demonstrating the increasing diffuse reflection of light toward larger film thicknesses. At a nominal thickness of 50 μm , the nanofoamed reflector is effectively opaque, and all incoming light is scattered (diffuse reflection).

2.3. Solar Cells with Nanoporous Reflectors

Finally, we attached the nanoporous reflectors to the solar cells, behind the rear PEDOT:PSS:AgNW electrodes. While the PEDOT:PSS:AgNW electrodes alone would be a perfect choice for semitransparent solar cells, the additional nanoporous reflectors warrant enhanced PCEs due to (partly) backscattered light. The thickness of the nanoporous reflector allows to tailor the PCE or, likewise, the translucency of the device as depicted on the right side of Figure 3. Notably, if used as a semitransparent solar cell, the nanoporous reflectors produce a certain haze on the transmitted light, depending on the actual thickness of the nanoporous layer, which renders this device concept particularly interesting for frosted window applications.

The solar cells and the thickness of the bulk-heterojunction were optimized for best PCEs in the absence of any reflector, i.e., a standard semitransparent OSC comprising a PEDOT:PSS:AgNW top electrode. At a PBDB-T:ITIC layer thickness of 150 nm, the devices achieved a PCE of $5.9 \pm 0.1\%$. **Figure 4a–c** depicts the transmittance, the absorbance, and the external quantum efficiency (EQE) of this and all other solar cells discussed in this work. In addition, **Table 1** summarizes the average visible transmission (AVT) of the solar cells with respect to the photopic response of the human eye.^[31] Each of the three characteristics is vastly dominated by the absorption of the PBDB-T:ITIC blend. All characteristics show severe flattening when nanoporous reflectors are employed, with the effect being most pronounced toward thicker reflectors which we attribute to the strong backscattering of light: the absorbance of rather weakly absorbed spectral regimes particularly benefits from the light-path elongation within the absorber layer by scattering. At the maximum of the OSC transmittance at 460 nm in Figure 4a, the transmittance of the full device can thus be varied from 21.3% at a reflector thickness of 10 μm down to 5.7% at a thickness of 50 μm . Notably, the absorption shows only negligible influence from thin-film interferences as it is often observed when using metal electrodes. Hence, the transparency color perception of the devices is almost invariant against electrodes with different reflection strength. Figure 4d depicts the $J-V$ curve of the solar cell under 1 sun equivalent illumination

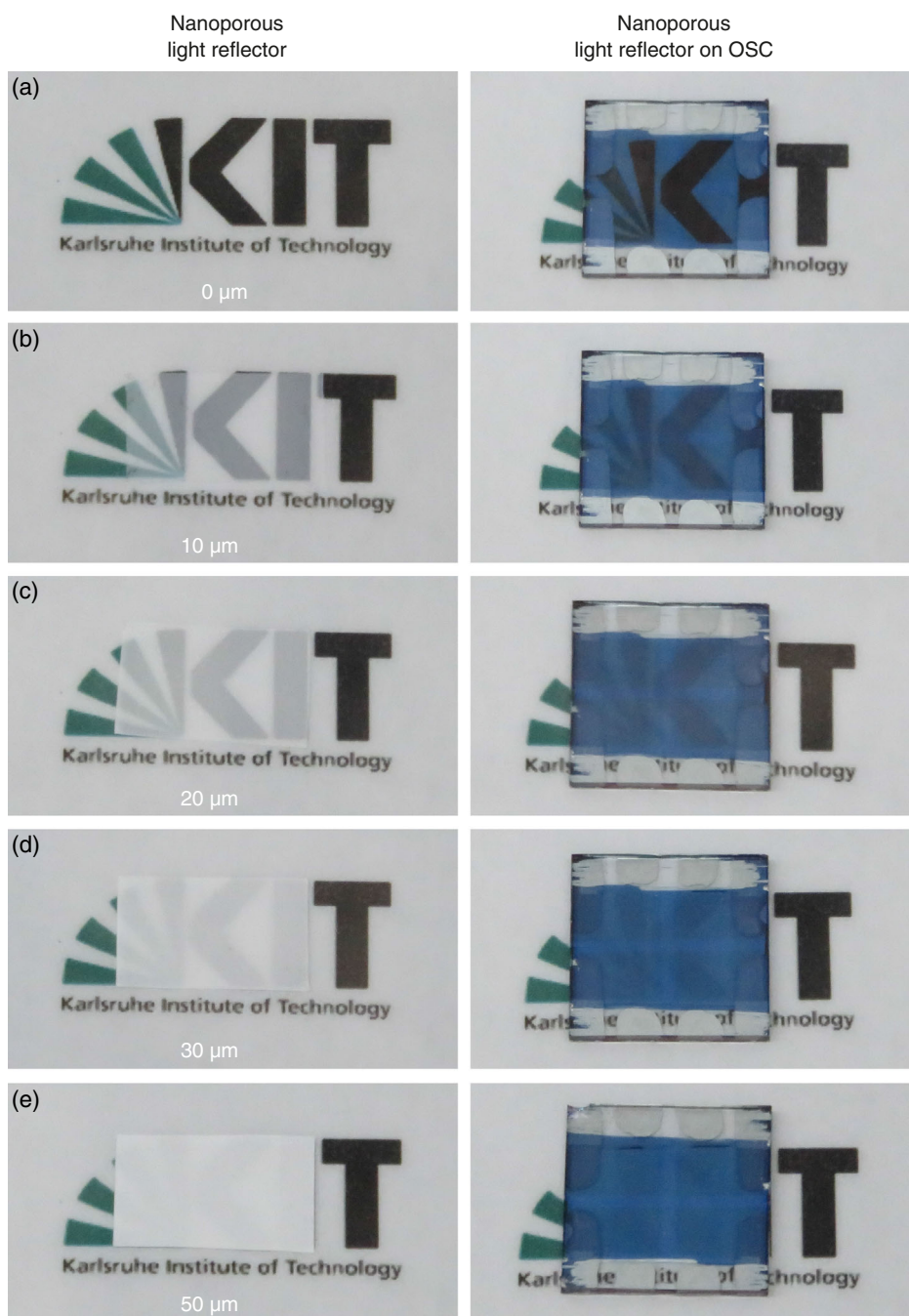


Figure 3. Photographs of nanoporous reflectors of different nominal thickness and hence of different translucency (left column). The right column demonstrates the transparency perception of OSCs with nanoporous reflectors attached. The logo is reproduced with permission from Karlsruhe Institute of Technology.

(ASTM AM1.5G) and in the dark. All key parameters of the solar cells are summarized in Table 1, i.e., the open-circuit voltage (V_{oc}), the short-circuit current density (J_{sc}), the fill factor (FF), and the PCE. Notably, all devices show excellent rectification behavior despite the use of polymer rear electrodes indicating best transport energy level alignments for negligible losses upon charge carrier extraction. Likewise, the matching FF of all devices shows no severe resistive losses within the polymer electrode. Attaching any of the nanoporous reflectors to the PEDOT:PSS:AgNW rear

electrode enhances the overall harvesting of light inside the device and hence improves the J_{sc} . The thicker the nanofoamed layers are, the higher is the J_{sc} and, consequently, the PCE. Finally, we attached the commercial 500 μm PMMA sample with best retro-reflection to the solar cell. Its light-harvesting properties equaled the solar cell with an Ag reflector attached. Due to the missing electric contact with the device, the Ag layer acted as a reflector only. The close-to-equal J_{sc} of the solar cells with the thick nanoporous reflector and the solar cells with the silver reflector

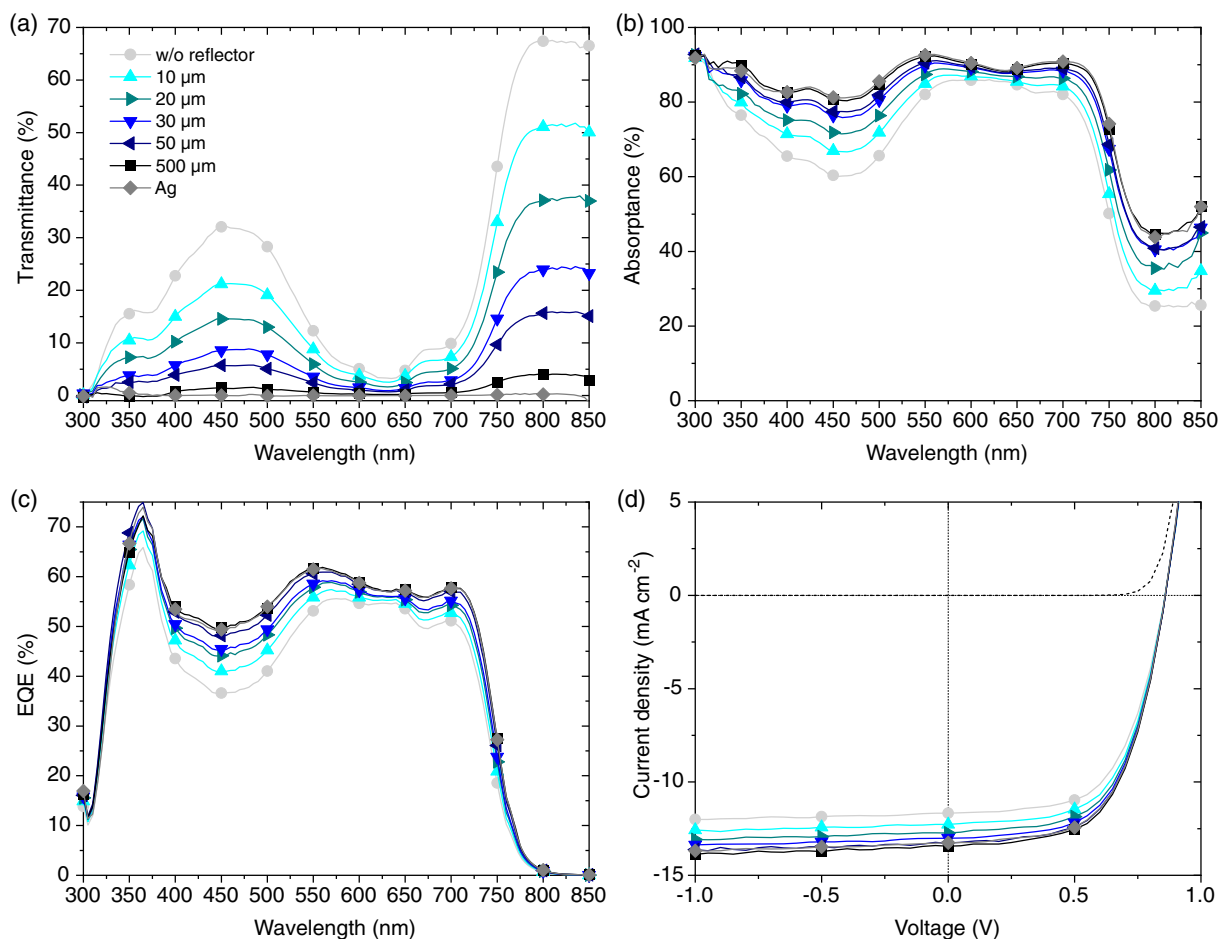


Figure 4. Optoelectronic properties of the PBDB-T:ITIC solar cells comprising PEDOT:PSS:AgNW rear electrodes, with and without nanoporous reflectors. For reference, a silver reflector was attached to the solar cell instead. a) Transmittance, b) absorbance, and c) EQE spectra of the devices measured under normal incidence. d) J - V curves of the solar cells measured under 1 sun equivalent illumination and in the dark (dashed line). For better readability, only one out of ten data points is marked with a symbol.

Table 1. Summary of the open-circuit voltage (V_{oc}), short-circuit current density (J_{sc}), fill factor (FF), power conversion efficiency (PCE), and average visible transmittance (AVT) of all solar cells explored in this work. The experimental uncertainties represent the standard deviations of at least four measurements of each sample.

Nominal reflector thickness	AVT [%]	V_{oc} [mV]	J_{sc} [mA cm^{-2}]	FF [%]	PCE [%]
0 μm	13.0	853 ± 4	11.7 ± 0.2	60 ± 2	5.9 ± 0.1
10 μm	9.1	854 ± 3	12.3 ± 0.2	60 ± 1	6.3 ± 0.1
20 μm	6.2	855 ± 3	12.8 ± 0.2	59 ± 1	6.5 ± 0.1
30 μm	3.6	855 ± 3	13.1 ± 0.2	59 ± 1	6.6 ± 0.1
50 μm	2.5	855 ± 3	13.3 ± 0.2	60 ± 1	6.8 ± 0.1
500 μm	0.6	855 ± 3	13.5 ± 0.2	59 ± 1	6.9 ± 0.1
Ag	0.0	854 ± 3	13.4 ± 0.2	60 ± 1	6.8 ± 0.1

demonstrate the excellent and almost lossless retro-reflection of light from the nanoporous reflectors.

3. Conclusions

We have demonstrated that the combination of polymer electrodes and reflective nanoporous polymer films from foamed PMMA can replace the common metal electrodes in thin-film (organic) solar cells. Using a rapid and cost-effective supercritical CO_2 foaming process, we have fabricated PMMA reflectors of different thicknesses in order to tailor the degree of reflectivity and translucency toward the requirements of different applications, including fully opaque solar cells. In addition, the scattering effects enhance light harvesting in spectral regions where the bulk-heterojunctions absorb only weakly. It produces a certain transparency color stability and a distinct frosted-window effect. While our approach was illustrated on a PBDB-T:ITIC bulk-heterojunction solar cell, it can be readily translated to other organic blends and even other thin-film PV technologies. In organic photovoltaics, this electrode configuration can be an interesting asset toward a sustainable and all-organic solar cell without incorporation of heavy metals or rare elements.

4. Experimental Section

Fabrication of Nanoporous Polymer Reflectors: Glass substrates ($2 \times 2 \text{ cm}^2$) were cleaned with acetone and isopropanol in an ultrasonic bath (5 min), and then exposed to oxygen plasma (2 min). Immediately after, PMMA resist (AR-P 672.11, ALLRESIST GmbH, $M_w = 0.95 \text{ MDa}$) was spin-coated, and thermally annealed on a hot plate (110°C , 5 min). The thickness of the PMMA films was tuned from nominally 10 to $50 \mu\text{m}$ by repeatedly spin coating the PMMA solution. The $10 \mu\text{m}$ layer was obtained by spin coating twice (1200 rpm , 30 s; 1700 rpm , 30 s). The other samples (20, 30, $50 \mu\text{m}$) were spin-coated repeatedly by three, five, and eight times, respectively (1000 rpm , 30 s). Then the PMMA films on glass were put in an autoclave vessel fed with pure CO_2 (80°C , saturation pressure 50 MPa , 1 min). Fast pressure quenching was initiated by quickly opening the outlet valve of the foaming apparatus. More details about the process and the growth mechanism of the pores are described in our previous work.^[30] Finally, the nanofoamed films were peeled off from their glass substrates. The $500 \mu\text{m}$ -thick PMMA reference sample ($M_w = 1.86 \text{ MDa}$) was purchased from Topacryl AG and subdued to microcellular foaming without further treatment.

Device Fabrication: Patterned indium tin oxide (ITO)-coated glass substrates ($R_{\square} = 13 \Omega \text{ sq}^{-1}$) were cleaned by sequential ultrasonication in acetone and isopropanol (10 min each). The ZnO electron extraction layers (30 nm) were doctor bladed in air (gap $150 \mu\text{m}$, speed 10 mm s^{-1} , 35°C) from nanoparticle dispersion by using a universal thin-film applicator (ZUA 2000, Zehntner). The ZnO nanoparticle dispersion was synthesized according to previous literature reports.^[32] Then the samples were thermally annealed on a hotplate (120°C , 10 min) and transferred into a nitrogen glove box for the remaining fabrication and characterization process. The light-harvesting polymer donor PBDB-T (synthesized according to the literature^[33]) and the molecular acceptor ITIC (1-Material) were dissolved (1:1 w/w, 20 mg mL^{-1}) in chlorobenzene (Sigma-Aldrich). The solution was stirred on a hotplate overnight (60°C), and 1,8-diiodooctane (0.25 vol%, DIO, Alfa Aesar) was added to the stock solution half an hour before deposition. Then the solution was doctor bladed (60°C , applicator gap $200 \mu\text{m}$, speed 20 mm s^{-1}) to form a 150 nm -thick bulk-heterojunction layer. The samples were thermally annealed on a hotplate (160°C , 10 min). For the top electrode, a poly(3,4-ethylenedioxythiophene):poly(styrenesulfonate) (PEDOT:PSS) formulation including dispersed silver nanowires (Clevios HYE, Heraeus Deutschland GmbH & Co. KG) was doctor bladed (60°C , applicator gap $200 \mu\text{m}$, speed 5 mm s^{-1}) and thermally annealed (120°C , 5 min) to yield a thickness of 70 nm . Then the PEDOT:PSS:AgNW layers were structured using dicing tape. The photoactive area of 0.105 cm^2 was defined by the cross section of the two electrodes. Finally, the reflectors were attached on the rear side of the device deliberately omitting refractive index matching oil since the oil would have damaged the HYE electrode. The reflectors were self-adhering. Only the $500 \mu\text{m}$ sample required additional fixing with tape. For reference, we fabricated a mock-silver-electrode (Ag, 100 nm , 99.9%, ChemPur) on glass that was sublimed in a vacuum chamber ($<0.1 \text{ mPa}$). When attached to the semitransparent solar cell in order to imitate a rear silver electrode, it was electrically isolated from the device by a $300 \mu\text{m}$ thin and highly transparent PMMA layer and fixed with tape.

Characterization: The cross-sectional micrograph of the nanoporous PMMA film shown in Figure 1b was obtained at an accelerating voltage of 1 kV on a scanning electron microscope (SEM; SUPRA 55 VP, Zeiss), after the sample was immersed into liquid nitrogen, broken to expose its nanoporous network, and covered with a thin gold layer. To determine the typical dimensions of the foamed nanopores, 100 pores were analyzed using ImageJ (software version 1.52a).

The reflectance spectra of the nanofoamed reflectors, before and after coupling to the OSC, were measured under close-to-normal (8°) light incidence employing an integrating sphere (Lambda 1050 UV/vis/NIR spectrometer, PerkinElmer).

The optoelectronic properties of the OSCs were measured using a shadow mask (0.105 cm^2). Current density–voltage (J – V) curves were measured with a source-measure unit (Keithley 2400, Keithley Instruments Corporation) under illumination from a Class AAA solar

simulator (Sciencetech AX LightLine with LA200 Homogenizing Optics, ASTM AM1.5G), and using a KG5 filtered silicon reference cell (91 150-KG5, Newport). For the EQE measurements, chopped monochromatic probe light was generated by a high-pressure xenon plasma lamp (450 W LSH601, LOT Oriel) and a monochromator (Omni- λ 300, LOT Oriel), including a set of wavelength filters (MSZ3122, LOT Oriel) and optics. The respective current densities were measured using a lock-in amplifier (DLPCA-S, Femto Messtechnik GmbH and eLockIn 203, Anfatec Instruments AG) synchronized with the chopped monochromatic probe light.

Acknowledgements

S.Y. and B.G. contributed equally to this work. The authors thank Holger Röhm (KIT) for preparing the device illustration in Figure 1. This work was conducted within the “PROPOLIS” project (HO 2273/12-1 and GO 2615/2-1) funded by the Deutsche Forschungsgemeinschaft (DFG) through program DFG-SPP 1839 “Tailored disorder”. G.G. acknowledges support from the Karlsruhe School of Optics and Photonics (KSOP). S.Y. and B.G. acknowledge scholarships from the China Scholarship Council (CSC). S.Y. acknowledges financial support from National Natural Science Foundation of China (grant no. 51735004) and China Postdoctoral Science Foundation (grant no. 2020M672618). A.C. thanks the Helmholtz program “Materials and Technologies for the Energy Transition” for support.

Open access funding enabled and organized by Projekt DEAL.

Conflict of Interest

The authors declare no conflict of interest.

Data Availability Statement

The data that support the findings of this study are available from the corresponding authors upon reasonable request.

Keywords

light scattering, nanoporous reflectors, organic solar cells, semitransparent films, supercritical CO_2 foaming

Received: August 6, 2021

Revised: October 7, 2021

Published online:

- [1] A. Colsmann, H. Röhm, C. Sprau, *Sol. RRL* **2020**, *4*, 2000015.
- [2] Y. Li, G. Xu, C. Cui, Y. Li, *Adv. Energy Mater.* **2018**, *8*, 1701791.
- [3] H. Jinno, K. Fukuda, X. Xu, S. Park, Y. Suzuki, M. Koizumi, T. Yokota, I. Osaka, K. Takimiya, T. Someya, *Nat. Energy* **2017**, *2*, 780.
- [4] L. Meng, Y. Zhang, X. Wan, C. Li, X. Zhang, Y. Wang, X. Ke, Z. Xiao, L. Ding, R. Xia, *Science* **2018**, *361*, 1094.
- [5] C. Sun, R. Xia, H. Shi, H. Yao, X. Liu, J. Hou, F. Huang, H.-L. Yip, Y. Cao, *Joule* **2018**, *2*, 1816.
- [6] D. Wang, R. Qin, G. Zhou, X. Li, R. Xia, Y. Li, L. Zhan, H. Zhu, X. Lu, H. L. Yip, H. Chen, C. Z. Li, *Adv. Mater.* **2020**, *32*, 1.
- [7] D. Wang, H. Liu, Y. Li, G. Zhou, L. Zhan, H. Zhu, X. Lu, H. Chen, C. Li, *Joule* **2021**, *5*, 945.
- [8] Q. Liu, Y. Jiang, K. Jin, J. Qin, J. Xu, W. Li, J. Xiong, J. Liu, Z. Xiao, K. Sun, S. Yang, X. Zhang, L. Ding, *Sci. Bull.* **2020**, *65*, 272.
- [9] J. Czolk, D. Landerer, M. Koppitz, D. Nass, A. Colsmann, *Adv. Mater. Technol.* **2016**, *1*, 1600184.

- [10] M. Koppitz, E. Wegner, T. Rödlmeier, A. Colsmann, *Energy Technol.* **2018**, *6*, 1275.
- [11] G. Xu, L. Shen, C. Cui, S. Wen, R. Xue, W. Chen, H. Chen, J. Zhang, H. Li, Y. Li, *Adv. Funct. Mater.* **2017**, *27*, 1605908.
- [12] F. Pastorelli, P. Romero-Gomez, R. Betancur, A. Martinez-Otero, P. Mantilla-Perez, N. Bonod, J. Martorell, *Adv. Energy Mater.* **2015**, *5*, 1400614.
- [13] D.-D. Zhang, X.-C. Jiang, R. Wang, H.-J. Xie, G.-F. Ma, Q.-D. Ou, Y.-L. Chen, Y.-Q. Li, J.-X. Tang, *ACS Appl. Mater. Interfaces* **2013**, *5*, 10185.
- [14] R. Betancur, P. Romero-Gomez, A. Martinez-Otero, X. Elias, M. Maymó, J. Martorell, *Nat. Photonics* **2013**, *7*, 995.
- [15] W. Zheng, X. Luo, Y. Zhang, C. Ye, A. Qin, Y. Cao, L. Hou, *ACS Appl. Mater. Interfaces* **2020**, *12*, 23190.
- [16] Y. Zhang, Z. Peng, C. Cai, Z. Liu, Y. Lin, W. Zheng, J. Yang, L. Hou, Y. Cao, *J. Mater. Chem. A* **2016**, *4*, 11821.
- [17] W. Cao, J. D. Myers, Y. Zheng, W. T. Hammond, E. Wrzesniewski, J. Xue, *Appl. Phys. Lett.* **2011**, *99*, 135.
- [18] Y. Galagan, M. G. Debije, P. W. Blom, *Appl. Phys. Lett.* **2011**, *98*, 16.
- [19] Z. Tang, A. Elfving, J. Bergqvist, W. Tress, O. Inganäs, *Adv. Energy Mater.* **2013**, *3*, 1606.
- [20] J. E. Cotter, R. B. Hall, M. G. Mauk, A. M. Barnett, *Prog. Photovoltaics Res. Appl.* **1999**, *7*, 261.
- [21] O. Berger, D. Inns, A. G. Aberle, *Sol. Energy Mater. Sol. Cells* **2007**, *91*, 1215.
- [22] A. Basch, F. Beck, T. Söderström, S. Varlamov, K. R. Catchpole, *Prog. Photovoltaics Res. Appl.* **2012**, *20*, 837.
- [23] B. G. Lee, P. Stradins, D. L. Young, K. Alberi, T.-K. Chuang, J. G. Couillard, H. M. Branz, *Appl. Phys. Lett.* **2011**, *99*, 064101.
- [24] S. Yu, J. Chen, G. Liang, X. Ding, Y. Tang, Z. Li, *Bioinspir. Biomim.* **2020**, *15*, 016003.
- [25] W. Zou, L. Pattelli, J. Guo, S. Yang, M. Yang, N. Zhao, J. Xu, D. S. Wiersma, *Adv. Funct. Mater.* **2019**, *29*, 1808885.
- [26] Y. Tang, Z. Li, G. Liang, Z. Li, J. Li, B. Yu, *Opt. Express* **2018**, *26*, 27716.
- [27] J. Syurik, G. Jacucci, O. D. Onelli, H. Hölscher, S. Vignolini, *Adv. Funct. Mater.* **2018**, *28*, 1706901.
- [28] J. Syurik, R. H. Siddique, A. Dollmann, G. Gomard, M. Schneider, M. Worgull, G. Wiegand, H. Hölscher, *Sci. Rep.* **2017**, *7*, 46637.
- [29] W. Zhao, D. Qian, S. Zhang, S. Li, O. Inganäs, F. Gao, J. Hou, *Adv. Mater.* **2016**, *28*, 4734.
- [30] S. Yu, B. Fritz, S. Johnsen, D. Busko, B. S. Richards, M. Hippler, G. Wiegand, Y. Tang, Z. Li, U. Lemmer, H. Hölscher, G. Gomard, *Adv. Opt. Mater.* **2019**, *7*, 1900223.
- [31] C. Yang, D. Liu, R. R. Lunt, *Joule* **2019**, *3*, 2871.
- [32] W. J. Beek, M. M. Wienk, M. Kemerink, X. Yang, R. A. Janssen, *J. Phys. Chem. B* **2005**, *109*, 9505.
- [33] D. Qian, L. Ye, M. Zhang, Y. Liang, L. Li, Y. Huang, X. Guo, S. Zhang, Z. A. Tan, J. Hou, *Macromolecules* **2012**, *45*, 9611.